Check for updates

Development of flexible PVDF/ BaTiO$_3$-MoS$_2$ polymer nanocomposites for energy harvesting and gas sensing applications

Hemalatha Parangusan[1], Dana Al-Sowaidi[2], El-Hassan Elhadrami[3], Deepalekshmi Ponnamma[4], and Jolly Bhadra[1,*] ◉

[1] *Qatar University Young Scientists Center (QUYSC), Qatar University, P.O. Box 2713, Doha, Qatar*

[2] *Department of Electrical Engineering, Qatar University, P.O .Box 2713, Doha, Qatar*

[3] *Department of Chemical Engineering, Qatar University, P.O. Box 2713, Doha, Qatar*

[4] *Materials Science and Technology Program, Department of Mathematics, Statistics and Physics, College of Arts and Sciences, Qatar University, Doha 2713, Qatar*

ABSTRACT

The need for flexible and wearable devices is quite great in the modern era of advanced electronics and the Internet of Things (IoT). Here, we present a poly(vinylidene fluoride) (PVDF)/Barium Titanate–Molybdenum Disulfide (BaTiO$_3$–MoS$_2$) composite-based flexible piezoelectric nanogenerator (PENG) with an improved electroactive phase. The electroactive, β-phase of the PVDF is shown to increase with the addition of BaTiO$_3$–MoS$_2$ fillers as a result of the filler's good interfacial interaction with the polymer matrix. The improved electroactive phase in the PVDF matrix was confirmed by the X-ray diffraction method and FTIR analysis of the composite films. The uniform dispersion of filler particles in the polymer matrix was confirmed by a scanning electron microscopy analysis. The developed piezoelectric nanogenerator device generated peak-to-peak output voltage of 4.9 V with a high dielectric constant of 22 and a low dielectric loss of 4.7. The fabricated gas sensor can perform at room temperature and exhibits good gas sensing performance toward the NH$_3$ gas. It was found that, compared to all other samples, the composite PVDF/BaTiO$_3$–MoS$_2$ films had a high level of sensitivity. Additionally, the composite films showed response and recovery times of 11 and 17 s. The composite based on PVDF/BaTiO$_3$–MoS$_2$ is a suitable material for NH$_3$ sensor applications.

Address correspondence to E-mail: jollybhadra@qu.edu.qa

🍏 Springer

1 Introduction

Considering the importance of the energy problem and environmental pollution, it is essential to develop and incorporate sustainable, renewable energy sources in order to meet human demand and achieve socioeconomic environmental performance. There has been an enormous demand recently for monitoring and controlling these pollutants because ammonia (NH_3) is one of the most common air pollutants with a significant impact on the ecosystem. It is a very dangerous gas that is used in many industrial and domestic uses, such as the production of biodiesel, synthetic fiber, complex fertilizers, and dyes [1]. Additionally, NH_3 is a polluting gas that is hazardous to human health. It can damage the skin, eyes, and respiratory system with prolonged exposure to low amounts of NH_3 (less than 50 ppm) [2]. Therefore, the detection of NH_3 in various firms has raised serious concerns. Commercial NH_3 sensors, however, require a connected external power source, which decreases their value as a portable device and limits them from meeting the low power and self-powered criteria of today's internet of things. As a result, a reliable and simple self-powered gas sensor is needed to detect NH_3 at room temperature. Future wearable technology applications will require smart sensors with outstanding durability and self-powered features. Due to the smaller power requirements of small electronic components, energy harvesting via mechanical vibrations has drawn more interest in recent years. Particularly, self-powering systems based on the principle of piezoelectric nanogenerators, which harvest energy from mechanical vibrations, have drawn a lot of interest [3]. The efficiency of piezoelectric power harvesting devices, which are mostly based on ceramics like lead zirconate titanate (PZT) or barium titanate ($BaTiO_3$), ZnO, Ni–$CoTiO_3$, $NaNbO_3$, are currently being improved with significant effort. However, when subjected to high frequency cyclic loading, piezoceramics can develop fatigue cracks, which limits their use in flexible and wearable technology [4–9]. Due to its high degree of flexibility, lightweight, ease of production, and long-term stability under powerful electric fields, PVDF is a piezoelectric polymer with particular potential [10]. Furthermore, studies have demonstrated that doping was a successful method for enhancing the PVDF piezoelectric characteristics, which became essential for enhancing the performance of piezoelectric sensors. Fu et al. [11] reported that the incorporation of multi-walled carbon nanotubes (MWCNT) to PVDF surface charge density nanofibers, led to an increase in output performance of the nanogenerator. It has been found that a piezoelectric (PVDF)/$BaTiO_3$ nanocomposite can be used to develop very flexible piezoelectric nanogenerators with an highest piezoelectric output voltage [12].

Several polymeric materials, semiconductors, and inorganic/organic composites have been employed as sensing materials, with each having its own unique sensing principles and mechanisms. However the main advantage of polymer-based gas sensors is that they are inherently flexible [13–15]. Polyvinylidene fluoride (PVDF) is one of the polymers that has been studied in more detail as a sensing polymeric film. The flexibility of the film makes them very useful. However, the usage of polymer-based materials as an electron-transporting medium in electronics requires the incorporation of one or more nanoparticles [16]. Chen et al. [17] studied PANI/PVDF polymer nanocomposites membranes and reported response value of 24.5% and 2.6% to 1 ppm and 0.1 ppm NH_3 at room temperature. In the last few years, MoS_2 based gas sensor material has been considerable interest due to their ability to detect gas at significantly lower temperatures compared to metal oxides. These properties make them perfect for use as sensors on flexible substrates [18]. Furthermore, MoS_2 based gas sensors have weak recovery, slow response time, and low sensitivity at ambient temperature [19]. Numerous techniques have been employed to enhance the sensing capabilities, including ligand conjugation, chemical doping, exposing the MoS_2 edge sites, and incorporating inorganic nanomaterials. Among other nanomaterials, barium titanate ($BaTiO_3$) is one of the most important technologically because of its high dielectric constant and ferromagnetic response, which is considered to be highly beneficial for the development of the electronic industry [20]. In this work, we report on the synthesis of PVDF/ $BaTiO_3$–MoS_2 composites films for the purpose of NH_3 detection. In addition, the developed PVDF/$BaTiO_3$–MoS_2 composite films acts as a piezoelectric nanogenerator. The electrical characterization of as-prepared PVDF/$BaTiO_3$–MoS_2 nanogenerators was studied. The maximum peak-to-peak output voltage for PVDF/$BaTiO_3$–MoS_2– based piezoelectric nanogenerator reached 4.9 V, which is greater than the pure PVDF, PVDF/$BaTiO_3$, and PVDF/MoS_2 samples. The incorporation of $BaTiO_3$–MoS_2 composite enhances the piezoelectric and gas sensing

properties. These wide-ranging properties extend the potential application of PVDF/BaTiO$_3$–MoS$_2$ based composite film toward energy harvesting, low power electronics, and gas sensor.

2 Experimental

2.1 Materials and methods

Barium acetate, Titanium (IV) n-butoxide, ethanol, and Bulk Molybdenum disulfide were purchased from Sigma Aldrich. Poly(vinylidenefluoride) (PVDF) pellets were purchased from Sigma-Aldrich. The polymer was dissolved in acetone and N, N-dimethylformamide (DMF) (BDH Chemicals, Qatar).

2.2 Synthesis of MoS$_2$ flakes

Utilizing the weak van der Waals force existing between the bulk MoS$_2$ layers, we synthesized a few-layered MoS$_2$ from its bulk powder. In brief, 30 mg bulk MoS$_2$ powder was taken in a 100 ml glass vial containing 50 ml of DMF (N,N-Dimethylformamide) solution. The solution was bath sonicated for 12 h at room temperature. Final solution was then centrifuged at 5000 rpm for 10 min to remove the aggregates and un-exfoliated bulk MoS$_2$ particles.

2.3 Synthesis of pure BaTiO$_3$ and BaTiO$_3$/MoS$_2$ composite

A simple chemical process was used to prepare pure BaTiO$_3$ and BaTiO$_3$/MoS$_2$ composites. For the synthesis of pure BaTiO$_3$, first, 0.04 M Titanium (IV) n-butoxide and then 0.04 M barium acetate were dissolved in ethanol. The two liquids were then vigorously stirred together for two hours to prepare a homogenous mixture. The KOH solution was added to maintain the pH at 13 (0.1 M). The precipitate was then dried for 6 h at 80 °C. after being washed with ethanol and distilled water. Then, the as-prepared nanoparticles were calcined under air at 500 °C for 2 h.

The typical method used to prepare BaTiO$_3$/MoS$_2$ composites is as follows: Under vigorous stirring, the 0.04 M of Barium acetate/Titanium n-butoxide solutions was added to a 10 mL of few-layered MoS$_2$ solution. The resulting suspension was stirred for an hour. The KOH solution was added to maintain the pH at 13 (0.1 M). The precipitate powder was washed with ethanol and distilled water throughout the filtration process. The resultant precipitate was then dried in a vacuum oven at 80 °C. Finally, the prepared BaTiO$_3$/MoS$_2$ particles were calcined for two hours at 500 C.

2.4 Synthesis of PVDF and its composites

PVDF solution was prepared by the addition of 2 g PVDF pellets to a 1:1 mixture of DMF and acetone (15 ml solvent) and stirred for 3 h at 70 °C. The pure BaTiO$_3$, MoS$_2$, and BaTiO$_3$/MoS$_2$ (1wt%) nanopowders were dispersed in the same solvent mixture (5 mL) and then sonicated for 2 h. The filler solution and PVDF solutions were then mixed together. The whole mixture was magnetically stirred over the night to achieve the uniform dispersion. The well-dispersed PVDF nanocomposite solution was then casted into a clean glass plate.

To remove any remaining solvent, the fabricated films were kept for a few hours in a hot-air oven at 80 °C. Figure 1 depicts the process for developing PVDF composites with BaTiO$_3$/MoS$_2$ filler composites.

2.5 Device fabrication and characterization methods

The phase structure of the materials was identified using a powder X-ray diffractometer (Empyrean, Panalytical, UK). A thermogravimetric analysis (TGA) (4000) by Perkin–Elmer used to evaluate the thermal properties. Utilizing an FTIR, PerkinElmer Spectrum 400, in transmission mode, the phase shift in polymer
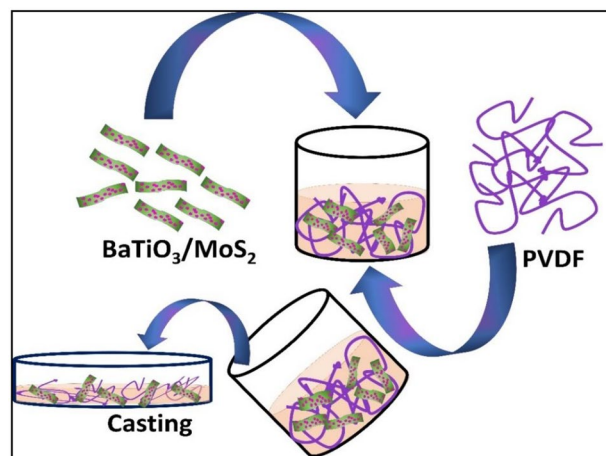

Fig. 1 Illustrates the fabrication of polymer nanocomposites schematically

nanocomposites was studied. Scanning electron microscopy (Nano-SEM Nova 450, FEI) was used to study the surface morphology of the nanocomposite films. Under room temperature, the broadband dielectric spectroscope GMbH concept 40 was used to determine the samples' dielectric characteristics as a function of frequency. Prior to conducting the piezoelectric experiments, the composite films were coated with silver paste to prepare a piezoelectric nanogenerator. In order to make electrical connections, Cu wires were attached with silver paste to the top and bottom of the composite films. A particular assembled set up, which included a resistance box, amplifier, vibrating shaker, frequency generator, and data gathering system, was used to conduct the piezoelectric studies. The sample was subjected to a specific force (2.5 N) in a longitudinal direction, and a computer analyzed the resulting power generation. Re-patterned interdigitated ITO (Indium Tin Oxide)/glass substrates (S161) were purchased from Ossila to fabricate the sensing device. On the glass substrate, ITO is 100 nm thick. Five ITO-based interdigitated sensor electrodes are built into each 20 mm × 15 mm substrate (extra data file), and each interdigitated sensor electrode is made up of three 30 mm x 50 m channels. The ITO/glass substrate is repeatedly cleansed in acetone and deionized water in an ultrasonic bath for 10 min prior to applying the sensing materials. Investigating the characteristics of

gas sensing was carried out using an integrated experimental device. The system included a Keithley 2400, a source meter, a measurement chamber, and measuring apparatus. The electrical characteristics of the manufactured sensors were measured by the Keithley 2400.

3 Result and discussion

3.1 Morphology and structure of BaTiO$_3$/MoS$_2$ composite

The powder X-ray diffraction patterns of pure BaTiO$_3$, MoS$_2$, and BaTiO$_3$/MoS$_2$ composite are displayed in Fig. 2(a–c). The peaks observed at $2\theta = 22.0°$, 24.1°, 31.4°, 38.8°, 45.0°, 50.8°, and 56.1°, respectively, correspond to the diffraction peaks of BaTiO$_3$, whereas the peaks of MoS$_2$ are corresponding to the standard diffraction data of MoS$_2$ hexagonal phase (JCPDS No.37-1492) [21, 22]. The XRD pattern of BaTiO$_3$/MoS$_2$ composite shows the distinct peaks for both BaTiO$_3$ and MoS$_2$, which confirms the formation of the composites structure.

FE-SEM images of the pure BaTiO$_3$, MoS$_2$, and BaTiO$_3$/MoS$_2$ composites are presented in Fig. 3(a–c). Figure 3a shows the pure BaTiO$_3$ sample, it consists of spherical nanoparticles with less agglomeration. As shown in Fig. 3b, pure MoS$_2$ nanosheets provide a

Fig. 2 X-ray diffraction pattern of (**a**) pure BaTiO$_3$, (**b**) MoS$_2$, and (**c**) BaTiO$_3$/MoS$_2$ composite
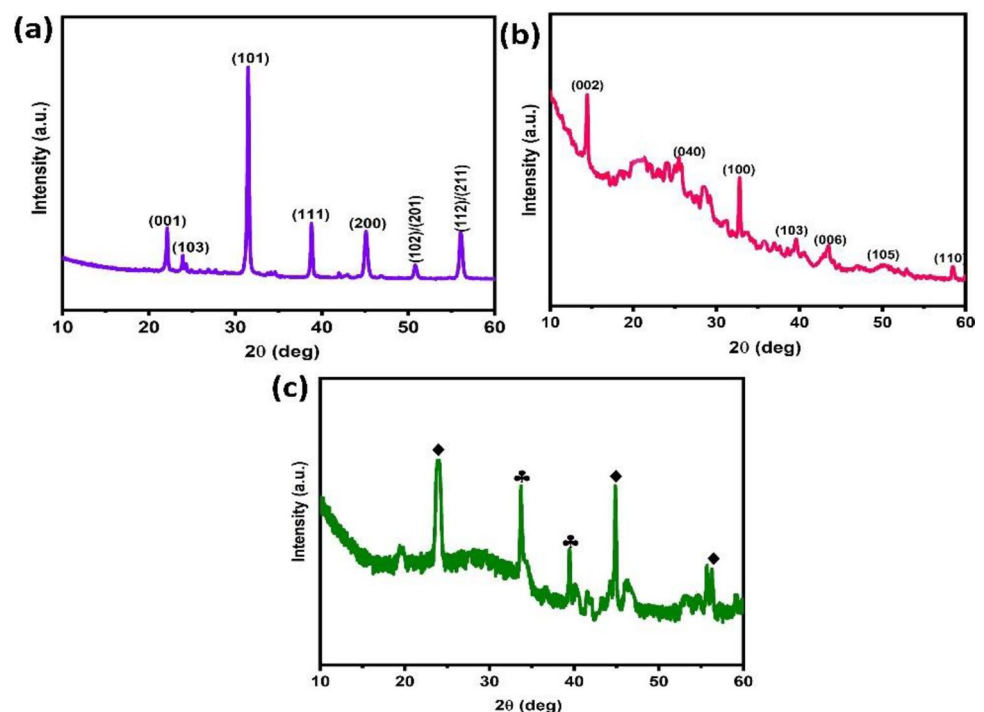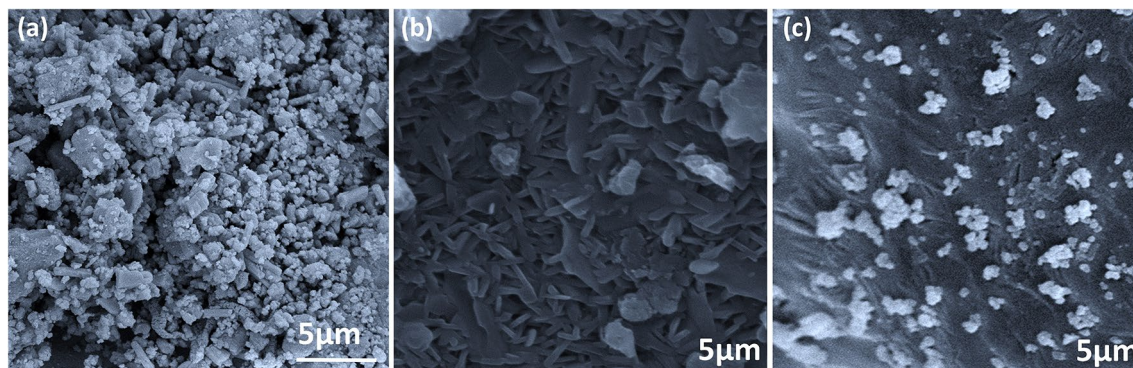
Fig. 3 FE-SEM images of (**a**) pure BaTiO$_3$, (**b**) MoS$_2$, and (**c**) BaTiO$_3$/MoS$_2$ composite

good substrate for nanoparticle attachment. Figure 3c shows the morphology of BaTiO$_3$/MoS$_2$ composite sample. The results indicate that the SEM images show the nanosheets decorated with BaTiO$_3$ nanoparticles in the composite. The sheets were interconnected with nanoparticles, which allows gas to move into the inside of the material and enhances NH$_3$ gas sensing. The main factor contributing to the enhanced gas sensing abilities of the BaTiO$_3$/MoS$_2$ composites is the increased oxygen vacancy [23]. Due to the p-n heterojunction formed at the interfaces between n-type BaTiO$_3$ and p-type MoS$_2$, electrons can easily transfer from the BaTiO$_3$ to MoS$_2$ to form abundant oxygen vacancies [24]. These oxygen vacancies act as the electronic charge carriers that increase the composite's conductivity. They may be absorbed in oxygen molecules and develop more active sites which will capture electrons from BaTiO$_3$ and form oxygen ions to react with molecules of the target gas [25]. All these factors contribute to the excellent sensing properties of BaTiO$_3$/MoS$_2$ composite based sensors to NH$_3$ gas at room temperature.

3.2 Structure and morphology of PVDF and its nanocomposites

Figure 4 (a, b) shows the XRD and FTIR spectra of pure PVDF and its nanocomposites. Figure 4a shows the XRD spectra of PVDF and its composites. The crystalline α-phase of the polymer is represented by the diffraction peaks observed at $2\theta = 18.6°$ (020) and 26.4° (110). The peak at 20.6° (200/110) corresponds to the crystalline planes of β-phase [26]. When nanofillers were added, only the β-phase increased and the diffraction peak for

the PVDF's α-phase at $2\theta = 18.6°$ decreased. Due to the strong O–H. F–C hydrogen bond interaction at the PVDF/BaTiO$_3$–MoS$_2$ interfaces, the enhanced β-phase was predominantly attributed to the presence of nanofillers performing as nucleating sites. The XRD data show that the addition of nanofillers substantially enhances the β-phase formation of the nanocomposite.

FTIR is an effective technique for examining the exact phase development and chemical structure of piezoelectric polymers and its nanocomposites. Figure 4b shows the FTIR spectra for the pure PVDF and its composites. The three different characteristic absorption bands in the FTIR spectra correspond to the nonpolar α-, polar β-, and γ-phases of pure PVDF. Vibrational bands observed at 1380, 970, 760, and 610 cm^{-1} are attributed to the α-phase of the neat PVDF, whereas the bands at 882 and 1232 cm^{-1} are characteristic of the β-crystalline phases [27–29]. In addition, the peak at 835 and 1398 cm^{-1} corresponds to the γ-phase [30]. As can be seen from Fig. 4b, the intensity of the absorption peak of the nonpolar α phase gradually decreased for the PVDF/BaTiO$_3$-MoS$_2$ composite films and only those bands due to electroactive β and γ–phases were predominantly visible in the composite films. According to the FTIR results, incorporating BaTiO$_3$/MoS$_2$ nanofiller can gradually convert the non-piezoelectric α phase to the piezoelectric β-phase. This suggests that the nanofillers are essential for the nucleation and stabilization of the electroactive phases because of their surface charge and the –CH$_2$–/–CF$_{2\backslash}$– dipoles' of PVDF electrostatic interaction.

Additionally, the following equation is used to calculate the relative proportion of the β-phase F(β) [31].

$$F(\beta) = \frac{A_\beta}{1.26A_\alpha + A_\beta} \tag{1}$$

where A_β and A_α are the area of peaks at 882 and 760 cm^{-1}. Table 1 shows the significantly higher electroactive phase concentration of the PVDF/BaTiO$_3$-MoS$_2$ composite films when compared to the pure PVDF.

The surface morphologies of the PVDF, PVDF/BaTiO$_3$, PVDF/MoS$_2$, and PVDF/BaTiO$_3$-MoS$_2$ composites films are illustrated in Fig. 5a–d. As can be observed, the surface of the pure PVDF film shows smooth surface. It can be seen from Fig. 5c, that the MoS$_2$ layers are dispersed within the PVDF. In Fig. 5b and d, the PVDF/BaTiO$_3$-MoS$_2$ composite samples exhibited a uniform dispersion of BaTiO$_3$/MoS$_2$ composite in the PVDF matrix, without much agglomeration, as shown by the dotted red and green lines.

AFM measurement was performed in order to determine and compare the surface roughness of PVDF and its nanocomposite films. Figure 6(a–d)

Table 1 β-phase crystallinity data from FTIR spectra

Samples	β-phase crystallinity
PVDF	63.25
PVDF/BaTiO$_3$	65.42
PVDF/MoS$_2$	67.20
PVDF/BaTiO$_3$-MoS$_2$	68.21

illustrates the AFM images of PVDF, PVDF/BaTiO$_3$, PVDF/MoS$_2$, and PVDF/BaTiO$_3$–MoS$_2$ composites. Using Nanoscope Analysis software, surface images were obtained and the average height deviation from the mean plane (R_A) was determined. The Value of R_A was obtained as 4.300 nm, 6.227 nm, 4.392 nm, and 6.555 nm for PVDF, PVDF/BaTiO$_3$, PVDF/MoS$_2$, and PVDF/BaTiO$_3$–MoS$_2$ composites, respectively. These results clearly indicate that the PVDF/BaTiO$_3$-MoS$_2$ nanocomposite film has a more rough surface than PVDF film. As can be seen in Fig. 6c, the average roughness decreased in the PVDF/MoS$_2$ sample to 4.392 nm, indicating a smoother surface. The uniformity of MoS$_2$ nanosheet dispersion is indicated by the smoothness of the surface. Therefore, the AFM results confirms that addition of nanofiller to PVDF enhances its surface roughness, which will significantly increase its piezoelectric output. The increment in surface roughness causes higher friction, which leads to higher β-phase. The higher β-phase is responsible for enhanced piezoelectricity [32].

3.3 Thermal properties

Figure 7 shows the thermogravimetric and derivative thermogravimetric curves for PVDF and its nanocomposite films. PVDF composites are stable up to 419 °C, after that they begin to degrade. The decomposition temperature of PVDF is observed at 386.5 °C. The decomposition temperature increases to 441.3 °C and 408.9 °C with the addition of BaTiO$_3$ and MoS$_2$.
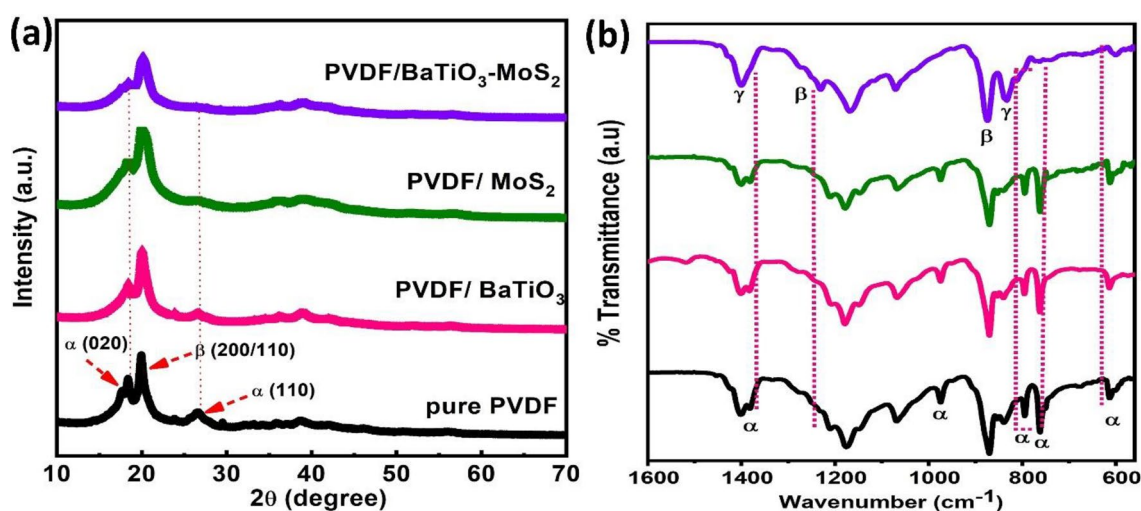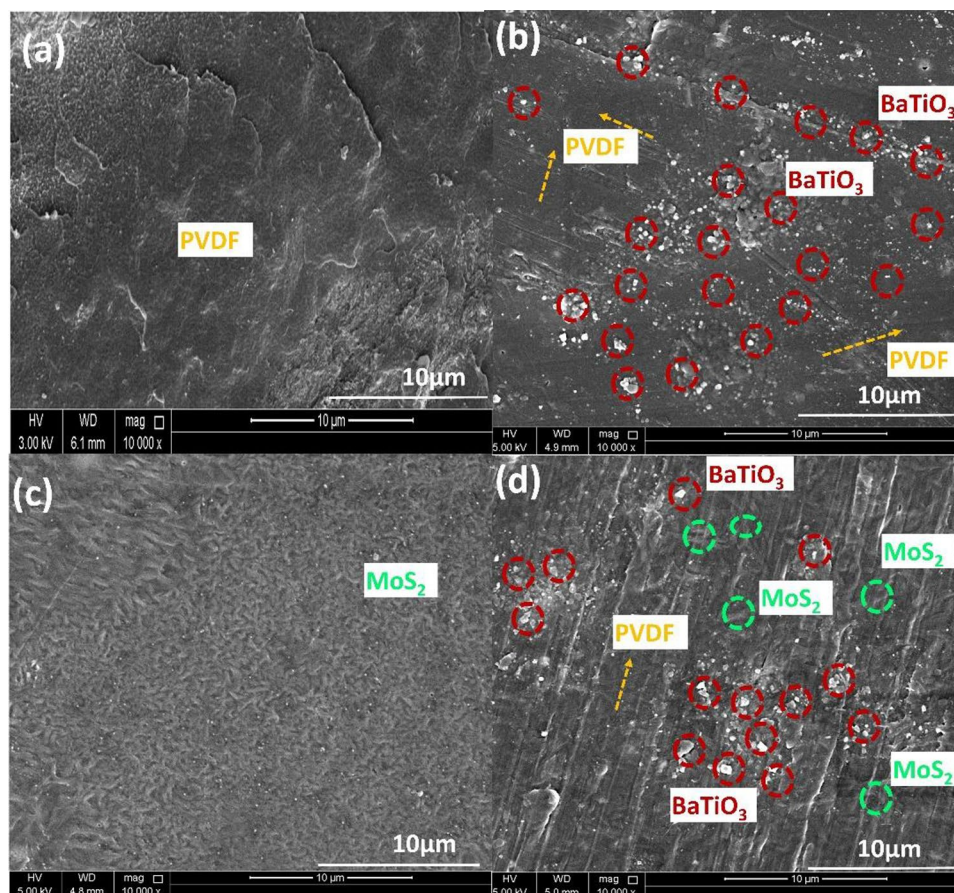

Fig. 4 a XRD spectra and **b** FTIR spectra of PVDF, PVDF/BaTiO$_3$, PVDF/MoS$_2$, and PVDF/BaTiO$_3$ -MoS$_2$ composite

Fig. 5 SEM images of **a** pure PVDF, **b** PVDF/BaTiO$_3$, **c** PVDF/MoS$_2$, and **d** PVDF/BaTiO$_3$–MoS$_2$ composite

However, the hybrid composite significantly increased thermal stability for the composite containing BaTiO$_3$/MoS$_2$ at 2 wt%, allowing it to reach up to 469 °C. This is because of the distribution of the filler materials within the polymer medium and the restricted movement of PVDF chains by the nanomaterials. Increased crystallinity, stronger attraction to polymer chains, and higher crosslink density are all results of uniformly distributed nanoparticles, and these all factors contribute to good thermal stability [33].

3.4 Dielectric properties

The composite system with a low dielectric loss and a high dielectric constant might be useful for energy storage applications. Investigating the dielectric properties of polymer nanocomposite systems is important since materials utilized in energy-producing devices must possess the ability to store energy [34]. Figure 8(a, b) displays the pure PVDF and its nanocomposites frequency-dependent dielectric constant and dielectric loss. As can be seen, the incorporation

of BaTiO$_3$–MoS$_2$ nano fillers increases the dielectric constant. The dielectric constant of the pure polymer was 8, while the dielectric constant of the PVDF/BaTiO$_3$–MoS$_2$ nanocomposite is 22. Table 2 shows a comparison of dielectric constant values of reported polymer-based composites. The dielectric constant increases as a result of the polarization of the BaTiO$_3$/MoS$_2$ particles as well as the interfacial polarization that takes place in a heterogeneous environment as a result of the charge accumulated at the PVDF and BaTiO$_3$/MoS$_2$ interface. In addition to the charge accumulation and short-range dipole dipole interactions at the PVDF/nanoparticle interface with the electrical field, the Maxwell–Wagner–Sillars (MWS) effect also contributes to the enhancement in the dielectric constant value for the nanocomposite. Therefore, the dispersion of nanoparticles and MWS effect were responsible for the improvement of dielectric constant for the composites samples. In addition to these effects, the dielectric constant value enhancement is also determined by the total interfacial area per unit volume of the nanoparticle. When the BaTiO$_3$–MoS$_2$
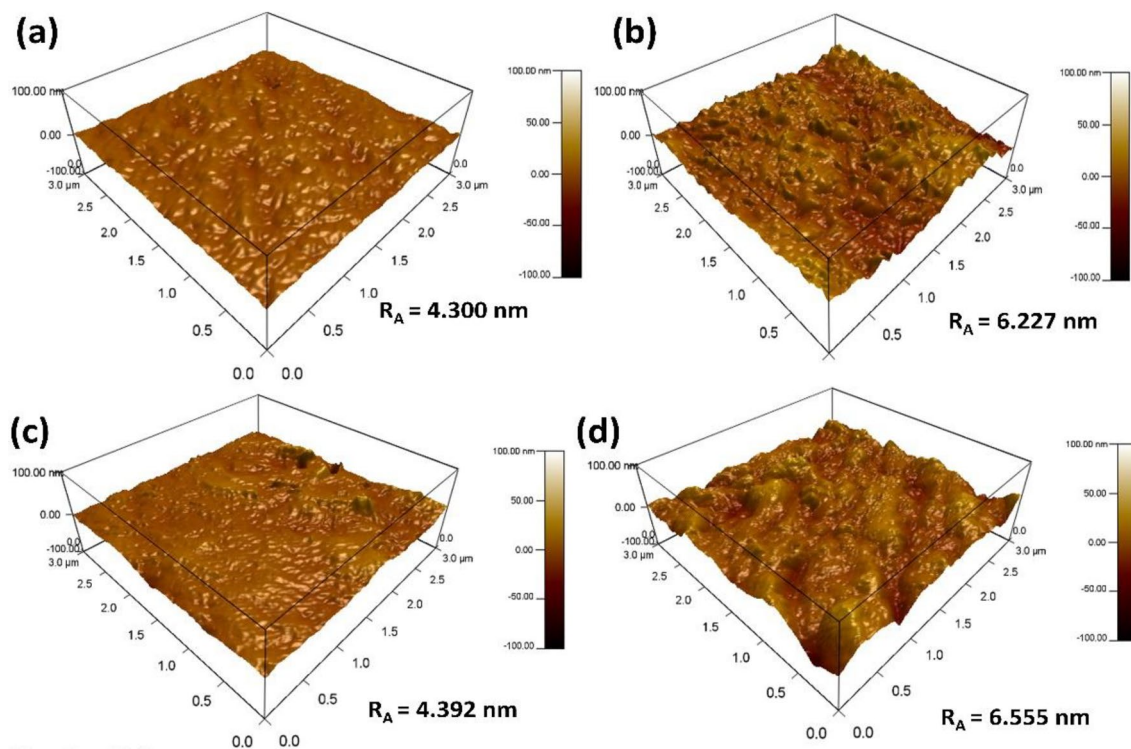
Fig. 6 AFM images of: **a** PVDF, **b** PVDF/BaTiO$_3$, **c** PVDF/MoS$_2$, and **d** PVDF/BaTiO$_3$ -MoS$_2$ composite
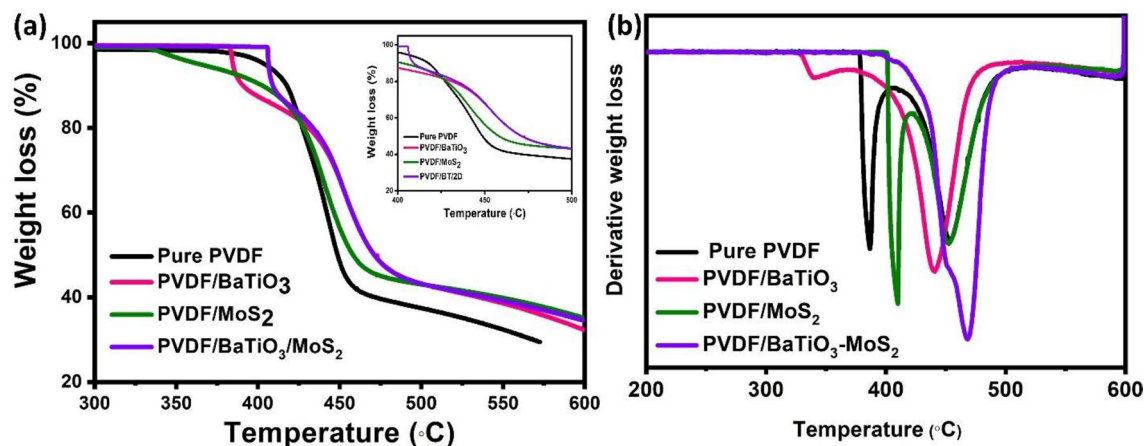

Fig. 7 **a** TGA and **b** DTA curves of pure PVDF, PVDF/BaTiO$_3$, PVDF/MoS$_2$, and PVDF/BaTiO$_3$ -MoS$_2$ composite

filler was simultaneously loaded into the nanocomposite, the dielectric loss value for the neat PVDF increased to 4.7 from 1.6. Due to interfacial polarization and space charge effects, the values for both the dielectric constant and the dielectric loss are high in the low frequency region [35]. Additionally, the dielectric constant decreases as a result of the reduced dipole mobility in the high frequency range. Because of their high dielectric constant values and low dielectric loss, the composites are suitable for application in energy storage and harvesting systems.

Figure 8c displays the samples conductivity as a function of frequency. The conductivity of all composites varies similarly with that of pure polymers. In the lower-frequency area, the conductivity values

Table 2 Comparison of dielectric constant of various polymer-based composites

Polymer matrix	Nanofiller	Dielectric constant	Nanocomposite preparation method	Ref
PVDF	xGnPs	2.08	Solution mixing process	[36]
PVDF-CTFE	PDA coated BT nanoparticles/BN nanosheets	11.7	Solution casting	[37]
PVDF	GPNs	11	Solution casting	[38]
PVDF-HFP	Dopamine modified urchin-like hierarchical structure of BT particles @TiO_2 nanowires	14.7	Solution casting	[39]
PVDF	BT-SiO_2	14.7	Solution casting	[40]
PVDF-HFP	BT-OPA	15	casting	[41]
PVDF	$BaTiO_3$–Mos_2	22	Solution casting	This work
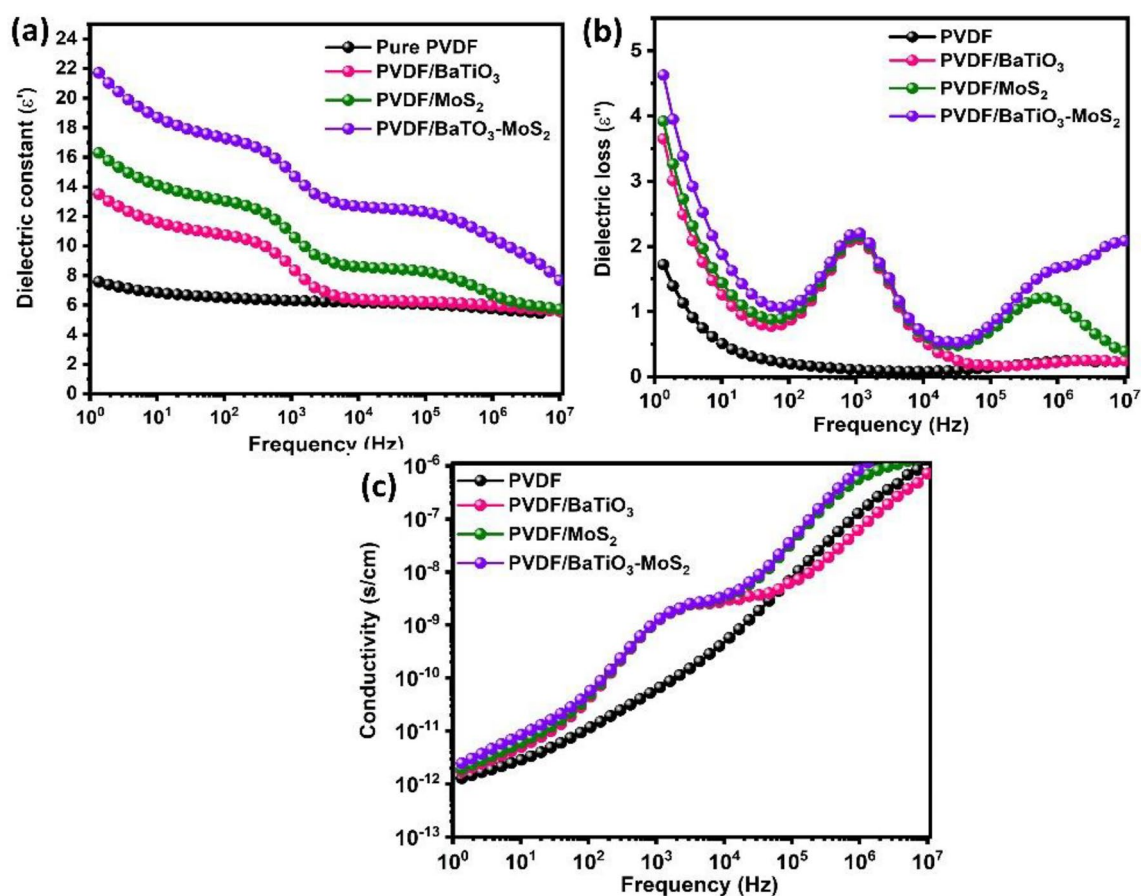
Fig. 8 **a** Dielectric constant, **b** Dielectric loss, and **c** Conductivity spectra of pure PVDF, PVDF/$BaTiO_3$, PVDF/MoS_2, and PVDF/$BaTiO_3$–MoS_2 composite

of the composites were in the range of 10^{-12} S/cm and increased with frequency. This suggests that the contact between PVDF and $BaTiO_3$–MoS_2 nanoparticles may also exhibit the Maxwell–Wagner–Sillars effect [42].

3.5 Piezoelectric property

For fabricating devices with the highest possible piezoelectric response, the films with the highest electroactive β-phase and dielectric values were chosen. Figure 9a shows the schematic of piezoelectric
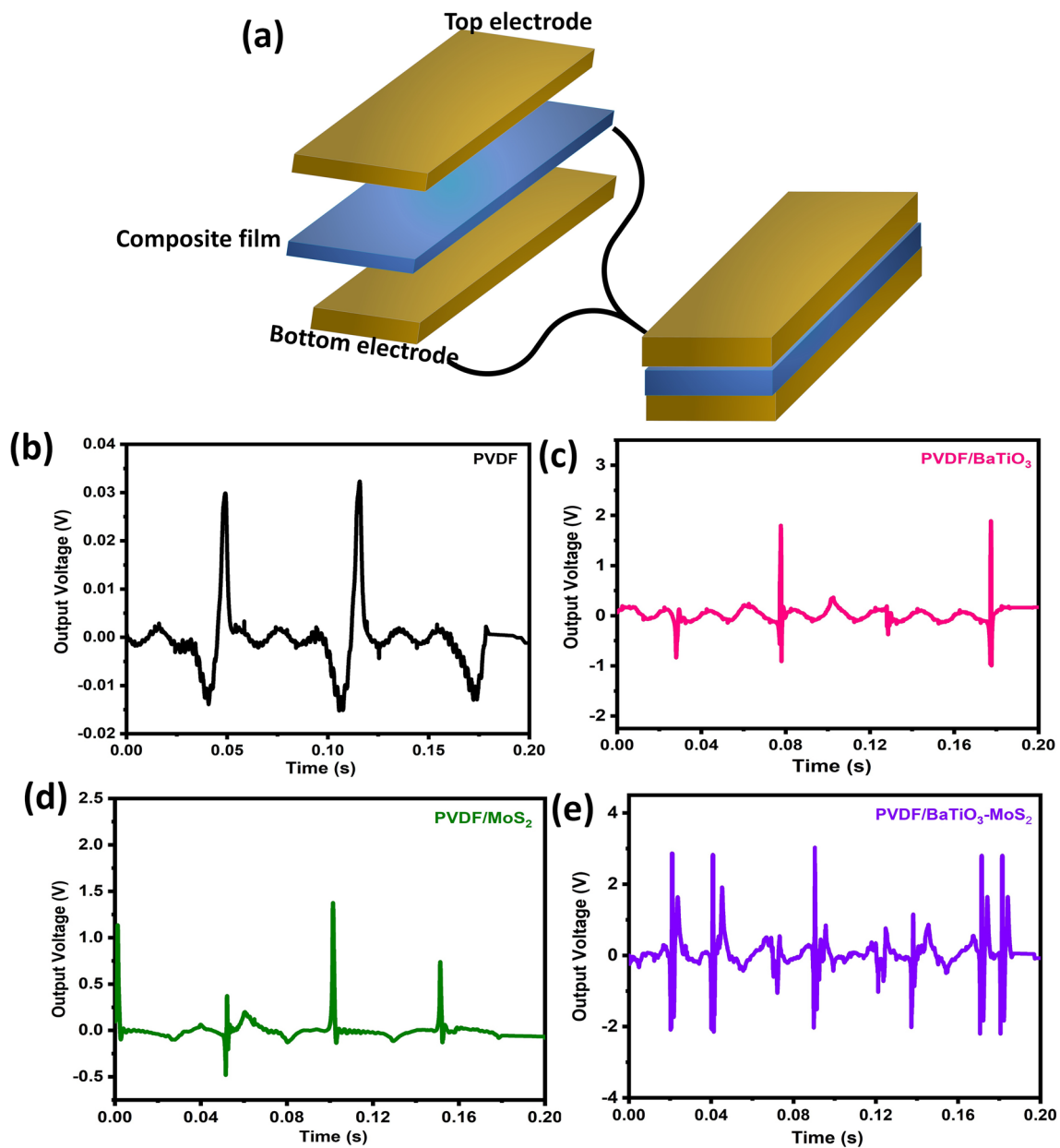
Fig. 9 **a** Diagram depicts several packing structures of PVDF/BaTiO$_3$–MoS$_2$ composites, **b** Values of the piezoelectric output voltage for pure PVDF, **b** PVDF/BaTiO$_3$, **c** PVDF/MoS$_2$, **d** PVDF/BaTiO$_3$-MoS$_2$ nanocomposites

nanogenerator devices fabricated by using the PVDF/BaTiO$_3$–MoS$_2$ composite films. Before performing the piezoelectric studies, the samples were coated with silver paste. Cu wires attached with silver paste, to provide electrical connections on the top and bottom of the composite films. Figure 9b shows output voltage as a function of load for devices using PVDF and its nanocomposite, clearly showing a higher output voltage for the BaTiO$_3$/MoS$_2$ composite sample. BaTiO$_3$/

MoS$_2$ filler content with a 2 N impact load produce a maximum peak-to-peak output voltage of 4.9 V, which is higher than that of pure PVDF. This can be attributed to the presence of piezoelectric BaTiO$_3$/MoS$_2$ filler in the nanocomposites.

In addition, the increase in output voltage is due to the relative proportions of polar β-phase present in the nanocomposites. It is evident from the XRD and FTIR results that the addition of BaTiO$_3$/MoS$_2$

nanofiller enhances the β-phase of PVDF. The composites $BaTiO_3/MoS_2$ strongly interacts with the $-CF_2-/-CH_2-$ dipoles of PVDF because of the presence of an oppositely charged influence on the surface [43]. In addition, by an application of mechanical force, the crystal structure of the PVDF/$BaTiO_3$–MoS_2 films were deformed and the external pressure creates a potential in the $BaTiO_3/MoS_2$ composites, which aligns the dipoles in the PVDF matrix. The findings indicates that, these type of nanocomposites are appropriate for use in self-charging battery separators, bridges, shoes, footpaths, and cars as pressure sensors [44].

By bending and stretching the samples, the mechanical flexibility and uniformity of the piezoelectric performance were also examined. Figure 10 shows the flexibility of the piezoelectric nanogenerator. The findings indicate that nanocomposite films may find useful in mechanical energy harvesting for flexible self-powering gadgets.

3.6 Gas sensing properties

In the present study, the PVDF/$BaTiO_3$–MoS_2 nanocomposite films were evaluated for its sensitivity. The experimental setup for sensor measurement is shown in Fig. 11a.

Figure 11b, c displays the nanocomposite films' sensitivity responses to 2 ppm of NH_3 at room temperature (RT). Figure 11b, c illustrates the resistance-changing behavior that can be attributed from the nanocomposite films adsorbing or desorbing different molecules. Figure 11b shows the sensitivity results for PVDF/$BaTiO_3$–MoS_2 at various NH_3 gas concentrations (0.5 ppm, 1 ppm, 1.5 ppm, and 2 ppm). It was observed that among all the nanocomposites, the samples with 1wt% $BaTiO_3/MoS_2$ composites loadings showed the greatest response to NH_3 at room temperature. These results showed that a higher absorption of NH_3 due to the nanocomposite films larger surface area. It has been shown that increasing the sensing material's surface area can increase the gas sensor's sensitivity.

The response time, a crucial sensor measurement, is the amount of time needed to reach 90% of the whole sensor response after exposure to the targeted gas (NH_3). When the target gas is removed, the recovery time is defined as the amount of time needed for the sensor to regain 90% of its initial signal [45]. For the efficient use of gas sensors, shorter recovery times are highly required. The process and recovery times for all samples are shown in Fig. 11c at 2 ppm NH_3. Compared to all the samples, PVDF/$BaTiO_3$–MoS_2 nanocomposite sensor showed a fast response and recovery time (11 and 17 s, respectively). The sensor typically responds quickly due to the adsorption of gas molecules [46]. One of the most significant factors in defining the sensors practical application is its long-term stability. Figure 11d displays the sensors stability toward 2 ppm NH_3 at room temperature. The stability of the PVDF/$BaTiO_3$–MoS_2-based sensors was observed. The results shows that the gas response did not significantly change throughout the course of the 25-day measurement. This means that the PVDF/

Fig. 10 The piezoelectric nanogenerator is depicted schematically, with the flexibility of nanocomposite films demonstrated by bending and twisting
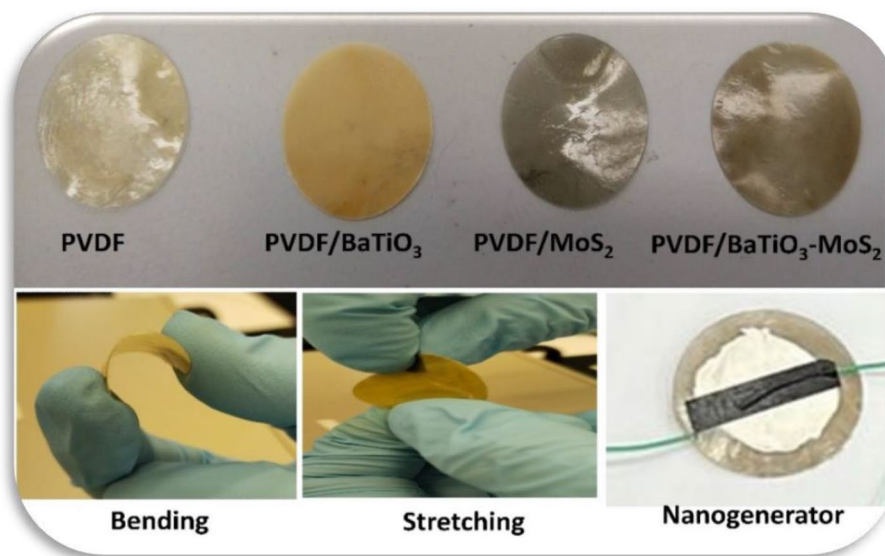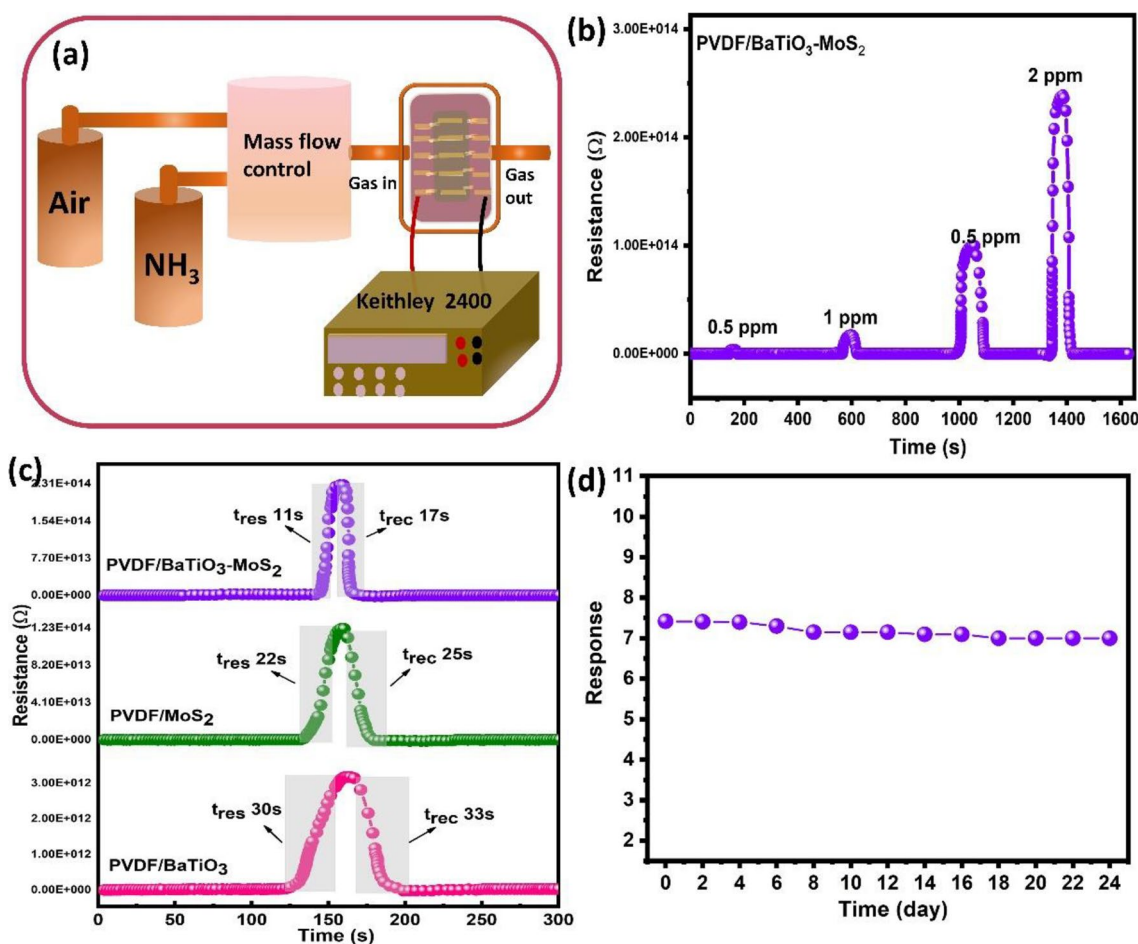
Fig. 11 a An illustration showing techniques to test NH_3 gas with a sensor, **b** Response of a room temperature, PVDF/$BaTiO_3$–MoS_2 composite sensor to NH_3 gas concentrations, **c** Response and recovery behavior of PVDF nanocomposites, **d** Long-term sensor stability at 2 ppm NH_3 at ambient temperature

$BaTiO_3$–MoS_2 nanocomposite sensors showed a fast response and good reproducibility. The connection between gas molecules and high binding energy sites, such as vacancies, defects, and oxygen-bearing functional groups found in the heterostructure, is generally responsible for the sensor's slow response, whereas the sensor's fast response is typically attributed to the adsorption of gas molecules at the lower binding energies.

4 Conclusion

In summary, we have successfully synthesized PVDF/$BaTiO_3$–MoS_2 composites film. Pure PVDF and its composites containing $BaTiO_3$, MoS_2, and $BaTiO_3$/MoS_2 fillers were fabricated by simple solution casting method. The enhancement in β-phase nucleation is confirmed by the FTIR and XRD analysis. Due to the Maxwell–Wagner (MW) interfacial polarization between the filler and PVDF matrix, it exhibited a maximum dielectric constant of 22. When mechanical vibrations were present, the fabricated piezoelectric nanogenerator was able to generate up to 4.9 V (peak-to-peak voltage). Additionally, the device has been tested as an ammonia gas sensor. The resistance values of the PVDF/$BaTiO_3$, PVDF/MoS_2, and PVDF/$BaTiO_3$–MoS_2 composites varied significantly from one another in the room temperature sensing studies. The PVDF/$BaTiO_3$-MoS_2 composite-based ammonia sensor exhibits a higher sensitivity when compared to the other composite samples.

Acknowledgements

Author contributions

DS and EH: Data collection, figures preparation, HP: Methodology, writing—original draft preparation, JB, DP: Writing—review and editing; JB: Funding acquisition, project administration. All authors read and agreed to the published version of the manuscript.

Funding

Data availability

Data will be made available on request.

Declarations

Conflict of interest The authors declare that they have no conflict of interest.

Consent to participate All authors have the consent to participate.

Consent for publication All authors have the consent to publish.

References

1. T. Huang et al., Fabrication of rigid and flexible SrGe 4 O 9 nanotube-based sensors for room-temperature ammonia detection. Nano Res. **11**, 431–439 (2018)

2. H.-Y. Li et al., Flexible room-temperature NH3 sensor for ultrasensitive, selective, and humidity-independent gas detection. ACS Appl. Mater. Interfaces. **10**(33), 27858–27867 (2018)

3. H. Parangusan, D. Ponnamma, M.A.A. AlMaadeed, Investigation on the effect of γ-irradiation on the dielectric and piezoelectric properties of stretchable PVDF/Fe–ZnO nanocomposites for self-powering devices. Soft Matter. **14**(43), 8803–8813 (2018)

4. X. Chen et al., High-performance piezoelectric nanogenerators with imprinted P (VDF-TrFE)/BaTiO3 nanocomposite micropillars for self-powered flexible sensors. Small. **13**(23), 1604245 (2017)

5. A. Sobhani-Nasab et al., Controlled synthesis of CoTiO 3 nanostructures via two-step sol–gel method in the presence of 1, 3, 5-benzenetricarboxylic acid. J. Cluster Sci. **26**, 1305–1318 (2015)

6. A. Sobhani-Nasab et al., Synthesis, characterization, and photovoltaic application of NiTiO 3 nanostructures via two-step sol–gel method. J. Mater. Sci.: Mater. Electron. **26**, 5735–5742 (2015)

7. M. Mansournia, S. Rafizadeh, S.M. Hosseinpour-Mashkani, Hydrothermal synthesis, characterization and light harvesting applications of zinc oxide nanostructures. J. Mater. Sci.: Mater. Electron. **26**, 5839–5846 (2015)

8. M. Mansournia et al., Novel room temperature synthesis of ZnO nanosheets, characterization and potentials in light harvesting applications and electrochemical devices. Mater. Sci. Engineering: C **65**, 303–312 (2016)

9. M. Mansournia, S. Rafizadeh, S.M. Hosseinpour-Mashkani, An ammonia vapor-based approach to ZnO nanostructures and their study as photocatalyst material. Ceram. Int. **42**(1), 907–916 (2016)

10. M. Sharma, J.K. Quamara, A. Gaur, Behaviour of multiphase PVDF in (1 − x) PVDF/(x) BaTiO 3 nanocomposite

films: structural, optical, dielectric and ferroelectric properties. J. Mater. Sci.: Mater. Electron. **29**, 10875–10884 (2018)

11. J. Fu et al., Highly durable piezoelectric energy harvester based on a PVDF flexible nanocomposite filled with oriented BaTi2O5 nanorods with high power density. Nano Energy. **52**, 391–401 (2018)

12. U. Yaqoob, A.I. Uddin, G.-S. Chung, A novel tri-layer flexible piezoelectric nanogenerator based on surface-modified graphene and PVDF-BaTiO3 nanocomposites. Appl. Surf. Sci. **405**, 420–426 (2017)

13. C. Liu et al., Transparent air filter for high-efficiency PM2.5 capture. Nat. Commun. **6**(1), 6205 (2015)

14. K.C. Persaud, Polymers for chemical sensing. Mater. Today. **8**(4), 38–44 (2005)

15. C. Wang et al., Metal oxide gas Sensors: sensitivity and influencing factors. Sensors. **10**(3), 2088–2106 (2010)

16. A.N. Mallya, R. Kottokkaran, P.C. Ramamurthy, Conducting polymer–carbon black nanocomposite sensor for volatile organic compounds and correlating sensor response by molecular dynamics. Sens. Actuators B **201**, 308–320 (2014)

17. W. Chen et al., Flexible room temperature ammonia gas sensor based on in suit polymerized PANI/PVDF porous composite film. J. Mater. Sci.: Mater. Electron. **31**, 11870–11877 (2020)

18. D. Burman, A. Sharma, P.K. Guha, Flexible large MoS 2 film based ammonia sensor. IEEE Sens. Lett. **2**(2), 1–4 (2018)

19. H. Li et al., Fabrication of single-and multilayer MoS2 film-based field-effect transistors for sensing NO at room temperature. Small. **8**(1), 63–67 (2012)

20. D. Hennings, M. Klee, R. Waser, Advanced dielectrics: bulk ceramics and thin films. Adv. Mater. **3**(7–8), 334–340 (1991)

21. D.-A. Zhang et al., High capacity and cyclability of hierarchical MoS2/SnO2 nanocomposites as the cathode of lithium-sulfur battery. Electrochim. Acta. **173**, 476–482 (2015)

22. M. Faraz, H.H. Singh, N. Khare, A progressive strategy for harvesting mechanical energy using flexible PVDF-rGO-MoS2 nanocomposites film-based piezoelectric nanogenerator. J. Alloys Compd. **890**, 161840 (2022)

23. M. Bao et al., Plate-like p–n heterogeneous NiO/WO3 nanocomposites for high performance room temperature 2 sensors. Nanoscale **6**(8), 4063–4066 (2014)

24. Y. Han et al., Design of hetero-nanostructures on MoS2 nanosheets to boost NO2 room-temperature sensing. ACS Appl. Mater. Interfaces. **10**(26), 22640–22649 (2018)

25. H. Long et al., High surface area MoS2/graphene hybrid aerogel for ultrasensitive NO2 detection. Adv. Funct. Mater. **26**(28), 5158–5165 (2016)

26. X. Liu et al., Polymeric nanofibers with ultrahigh piezoelectricity via self-orientation of nanocrystals. ACS nano. **11**(2), 1901–1910 (2017)

27. J. Xue et al., Evaluation of piezoelectric property of reduced graphene oxide (rGO)–poly (vinylidene fluoride) nanocomposites. Nanoscale. **4**(22), 7250–7255 (2012)

28. K. Oumghar et al., (2020) Enhanced piezoelectric properties of PVdF-HFP/PZT nanocomposite for energy harvesting application. in IOP Conference Series: Materials Science and Engineering. IOP Publishing

29. S.K. Karan, D. Mandal, B.B. Khatua, Self-powered flexible Fe-doped RGO/PVDF nanocomposite: an excellent material for a piezoelectric energy harvester. Nanoscale. **7**(24), 10655–10666 (2015)

30. X. Cai et al., A critical analysis of the α, β and γ phases in poly (vinylidene fluoride) using FTIR. RSC Adv. **7**(25), 15382–15389 (2017)

31. H. Parangusan, D. Ponnamma, M.A.A. Al-Maadeed, Stretchable electrospun PVDF-HFP/Co-ZnO nanofibers as piezoelectric nanogenerators. Sci. Rep. **8**(1), 754 (2018)

32. J. Dai et al., Preparation of Al2O3/PU/PVDF composite membrane and performance comparison with PVDF membrane, PU/PVDF blending membrane, and Al2O3/PVDF hybrid membrane. Desalination Water Treat. **57**(2), 487–494 (2016)

33. P. Irwin et al., (2003) Thermal and mechanical properties of polyimide nanocomposites. in 2003 Annual report conference on electrical insulation and dielectric phenomena. IEEE

34. A. Al-Saygh et al., Flexible pressure sensor based on PVDF nanocomposites containing reduced graphene oxide-titania hybrid nanolayers. Polymers. **9**(2), 33 (2017)

35. S. Nayak, T.K. Chaki, D. Khastgir, Development of flexible piezoelectric poly (dimethylsiloxane)–BaTiO3 nanocomposites for electrical energy harvesting. Ind. Eng. Chem. Res. **53**(39), 14982–14992 (2014)

36. Z. Wang et al., Ultrahigh dielectric constant and low loss of highly-aligned graphene aerogel/poly (vinyl alcohol) composites with insulating barriers. Carbon. **123**, 385–394 (2017)

37. Y. Xie et al., Enhancing breakdown strength and energy storage performance of PVDF-based nanocomposites by adding exfoliated boron nitride. Appl. Surf. Sci. **440**, 1150–1158 (2018)

38. J. Shang et al., Fabrication and enhanced dielectric properties of graphene–polyvinylidene fluoride functional hybrid

films with a polyaniline interlayer. J. Mater. Chem. A **1**(3), 884–890 (2013)

39. Q. Huang et al., Enhanced energy density in P (VDF-HFP) nanocomposites with gradient dielectric fillers and interfacial polarization. J. Alloys Compd. **696**, 1220–1227 (2017)

40. K. Yu et al., Poly (vinylidene fluoride) polymer based nanocomposites with significantly reduced energy loss by filling with core-shell structured $BaTiO_3/SiO_2$ nanoparticles. Appl. Phys. Lett. **102**(10), 102903 (2013)

41. C. Ehrhardt et al., BaTiO3–P (VDF-HFP) nanocomposite dielectrics—influence of surface modification and dispersion additives. Mater. Sci. Engineering: B **178**(13), 881–888 (2013)

42. R. Mahdi, W.A. Majid, Piezoelectric and pyroelectric properties of BNT-base ternary lead-free ceramic–polymer nanocomposites under different poling conditions. RSC Adv. **6**(84), 81296–81309 (2016)

43. B. Li et al., Wearable piezoelectric device assembled by one-step continuous electrospinning. J. Mater. Chem. C **4**(29), 6988–6995 (2016)

44. X. Xue et al., Hybridizing energy conversion and storage in a mechanical-to-electrochemical process for self-charging power cell. Nano Lett. **12**(9), 5048–5054 (2012)

45. T. Han et al., Rough SmFeO3 nanofibers as an optimization ethylene glycol gas sensor prepared by electrospinning. Mater. Lett. **268**, 127575 (2020)

46. S. Sardana et al., Self-powered monitoring of ammonia using an MXene/TiO2/cellulose nanofiber heterojunction-based sensor driven by an electrospun triboelectric nanogenerator. ACS Sens. **7**(1), 312–321 (2022)

Publisher's Note Springer Nature remains neutral with regard to jurisdictional claims in published maps and institutional affiliations.